

Can Transformer Memory Be Corrupted? Investigating Cache-Side Vulnerabilities in Large Language Models

Elias Hossain,^{1,*} Swayamjit Saha,² Somshubhra Roy,³ and Ravi Prasad⁴

¹College of Engineering and Computer Science, University of Central Florida, Orlando, FL 32816, United States

^{2,4}Department of Computer Science and Engineering, Mississippi State University, Mississippi State, MS 39762, United States

³Department of Electrical and Computer Engineering, North Carolina State University, Raleigh, NC 27695-7911, United States

*Corresponding author: mdelias.hossain@ucf.edu

Abstract: Even when prompts and parameters are secured, transformer language models can remain exposed because their key-value (KV) cache during inference constitutes an under-examined attack surface. We present *MTI* V.1, a modular framework that formalizes and implements Malicious Token Injection (MTI): cache-side perturbations applied to cached key vectors at selected layers and timesteps, with controllable magnitude and frequency (e.g., additive Gaussian noise, zeroing, and orthogonal rotations). We provide a theoretical analysis that upper-bounds how bounded cache perturbations propagate through attention, linking (i) logit deviations to the perturbation norm and query scaling, and (ii) shifts in attention and output distributions to these logit changes via standard softmax stability arguments under bounded-logit assumptions. Empirically, we show that *MTI* V.1 induces measurable distributional shifts and downstream performance degradation on GPT-2 and LLaMA-2/7B across synthetic prompts and standard NLP benchmarks. Extending to retrieval-augmented and agentic pipelines, we find that perturbations in post-retrieval layers can destabilize grounding and action selection. Collectively, these results motivate treating cache integrity as a first-class robustness boundary and position controlled KV perturbation as a reproducible experimental threat model for future research.

1. Introduction

Large language models (LLMs) have become foundational components of modern AI systems, enabling applications such as retrieval-augmented generation (RAG), autonomous agents, decision support, and long-horizon planning [1, 2, 3]. In deployed settings, their reliability depends not only on training-time alignment and prompt-level safeguards, but also on the integrity of inference-time execution. However, the robustness of internal inference-time state has received comparatively limited attention in the trustworthy AI literature.

A key mechanism enabling efficient inference in decoder-only transformers is the key-value (KV) cache, which stores intermediate attention representations across decoding steps. While essential for efficient inference, KV caching also introduces a persistent internal state that directly influences future predictions and has not been widely examined as a robustness boundary.

Cache-side perturbations differ fundamentally from prompt injection and training-time attacks. They operate entirely after tokenization and embedding, do not modify prompts or model parameters, and therefore bypass input-level filters and alignment checks. Even small, structured perturbations to cached representations can bias attention distributions and propagate through downstream predictions without triggering conventional safeguards. This observation motivates a central question for trustworthy AI: *Can inference-time cache corruption systematically undermine reliability, calibration, and grounding in modern LLM pipelines?*

To address this question, we introduce *MTI* V.1, a modular framework for studying cache-side perturbations during inference. The framework formalizes MTI as controlled modifications to cached key vectors at selected layers and timesteps, with tunable magnitude, frequency, and structure. We provide a theoretical analysis that bounds how norm-limited cache perturbations propagate through attention and affect next-token logits. Empirically, we show that cache corruption induces distributional shift, miscalibration, and task failure across GPT-2, LLaMA-2, and Gemma models, spanning language modeling, extractive question answering, summarization, retrieval-augmented generation, and agentic reasoning pipelines.

Our contributions are summarized as follows:

- We identify inference-time KV cache integrity as a critical and underexplored robustness boundary, and formalize cache-side perturbation as a principled threat model for trustworthy AI evaluation.
- We introduce a modular framework for controlled cache perturbation and provide theoretical bounds characterizing how bounded cache corruption propagates to attention distributions and output logits.
- We empirically demonstrate that cache perturbations induce distributional shift, miscalibration, and grounding failures across language modeling, retrieval-augmented generation, and agentic reasoning pipelines.
- We evaluate lightweight inference-time cache defenses that partially mitigate corruption with minimal runtime overhead.

2. Related Work

Prior research on transformer robustness and security broadly spans architectural efficiency, model integrity, and inference-time cache behavior. On the architectural side, Multi-Head Latent Attention (MLA) has emerged as an alternative to dense self-attention, introducing latent bottlenecks that reduce memory bandwidth while preserving long-context performance. DeepSeek-V2 first systematized MLA at scale [4], with subsequent iterations refining routing and optimization for improved efficiency and reasoning capabilities [5, 6], and TransMLA providing a formalized, research-oriented implementation [7]. In parallel, decoder-only Transformers universally rely on key-value (KV) caching to accelerate autoregressive decoding, as exemplified by GPT-3 [1], LLaMA-2 [2], Mistral-7B [8], Mixtral 8×7B [9], and the Qwen series [10]. While these systems emphasize throughput and scalability, the KV cache is typically treated as an implementation detail rather than a robustness or security boundary. These models are referenced to contextualize contemporary KV-cache usage and optimization trends, rather than evaluated empirically.

A separate line of work investigates attacks on model parameters themselves, including weight poisoning and backdoors in pretrained encoders [11], direct parameter editing to induce domain-specific harms in open LLMs [12], hardware-level bit-flip attacks under realistic fault models [13], and trojan insertion in code and clinical language models [14, 15], with recent surveys synthesizing these threat models and defenses [16]. More recently, attention has turned to the KV cache as a source of privacy and security risk during inference, including cross-session leakage in multi-tenant settings [17], timing-based side channels [18], prompt reconstruction attacks and cache obfuscation defenses [19], and restricted cache reuse policies [20]. However, existing cache-centric studies primarily focus on passive leakage rather than active manipulation. In contrast, this work treats the KV cache as a first-class adversarial surface and systematically studies how structured perturbations to cached keys induce distributional shift, miscalibration, and downstream failure during inference, bridging a critical gap between efficiency-driven caching mechanisms and robustness-oriented security analysis.

3. Cache Model and Threat Assumptions

Transformer decoders maintain a persistent *KV cache* during autoregressive decoding, storing projected representations of previously generated tokens to avoid recomputing attention over the full history. While essential for efficient inference, this cache also introduces a stateful internal memory that mediates future predictions. We treat the KV cache as a distinct inference-time robustness boundary and formalize the associated threat model below.

KV Cache Mechanism. At decoding step t , each layer projects token embeddings into queries, keys, and values, and computes attention via scaled dot products. Previously computed keys and values $\{k_j, v_j\}_{j=1}^{t-1}$ are stored in a cache and reused at subsequent steps, making cached representations persistent inputs to future attention computations.

Threat Model. We consider an adversary with inference-time access to the KV cache. The adversary cannot modify prompts or model parameters, but can perturb cached keys at selected layers and timesteps. Formally, at layer ℓ and position j ,

$$k_j^{(\ell)} \mapsto \tilde{k}_j^{(\ell)} = k_j^{(\ell)} + \delta_j^{(\ell)},$$

where $\delta_j^{(\ell)}$ is a corruption vector. Perturbations may be stochastic (e.g., Gaussian noise), destructive (e.g., zeroing), or structured (e.g., orthogonal rotations), and are controlled in magnitude and injection frequency. Unless stated otherwise, our theoretical analysis applies to non-adaptive, norm-bounded perturbations; optimized variants are evaluated empirically.

Scope and Relation to Prior Threat Models. This threat model captures settings where cache state can be modified during inference without altering inputs or weights, such as compromised runtimes or misconfigured shared deployments. Cache perturbations differ from prompt injection, which operates at the input interface, and from weight poisoning, which requires training-time access. Unlike cache leakage or side-channel attacks, which are passive, we study *active* manipulation of inference-time state. Accordingly, cache corruption represents a complementary robustness threat within the broader trustworthy AI landscape.

4. MTI V.1 Framework

We formalize *Malicious Token Injection (MTI)*, i.e., cache-side perturbations that modify stored attention key representations during inference without altering input tokens, prompts, or model parameters. The central observation underlying *MTI* V.1 is that attention weights are determined by inner products between queries and cached keys; consequently, even small but structured modifications to cached keys can bias attention distributions and alter downstream token predictions. Rather than defining a single attack, *MTI* V.1 specifies a family of cache perturbations controlled along three primary axes: (i) corruption magnitude, which determines the strength of the injected perturbation; (ii) injection frequency, which governs how often perturbations are applied across decoding steps; and (iii) layer placement, which specifies which transformer layers are targeted. This parameterization enables systematic exploration of cache sensitivity without assuming adversarial optimality.

Perturbation Classes. Within this framework, we study three canonical corruption mechanisms that span distinct modes of cache integrity violation. **MTI-Gaussian** injects additive noise sampled from $\mathcal{N}(0, \sigma^2 I)$ into cached keys, modeling stochastic corruption. **MTI-Zeroing** removes cached keys entirely, simulating catastrophic cache erasure and representing an extreme but informative failure mode. **MTI-Rotation** applies orthogonal transformations to cached keys, inducing structured yet norm-preserving perturbations that alter angular alignment with queries while preserving vector magnitude. Together, these mechanisms capture random noise, deletion, and structured misalignment, which represent three fundamental manifestations of cache perturbation during transformer inference.

Optimized Cache Perturbation. In addition to fixed-form perturbations, we also consider an optional optimization-based variant that computes cache perturbations designed to maximize an adversarial objective at inference time. This variant is used to characterize worst-case empirical behavior and is not assumed by the theoretical analysis. Specifically, Algorithm 1 describes an inner-loop procedure that iteratively updates a perturbation applied to a selected cached key by ascending the gradient of an adversarial loss, subject to a norm constraint. The procedure operates entirely on cached key representations and does not modify model weights, input prompts, or value vectors. All optimized perturbations are evaluated empirically and fall outside the scope of the formal bounds in Section 5, which apply exclusively to non-adaptive, norm-bounded perturbations.

Algorithm 1 OptimizePerturbation: Inner-loop adversarial perturbation

Require: model \mathcal{M} , current caches \mathcal{C} , query $q_t^{(\ell, h)}$, target position j , optimizer config \mathcal{O} (steps K , step size η , loss \mathcal{L}_{adv}), norm constraint ϵ

- 1: initialize perturbation $\delta \leftarrow \mathbf{0}$ (or small random noise)
- 2: **for** $k \leftarrow 1$ to K **do**
- 3: compute tentative key $\tilde{k} \leftarrow k_j + \delta$
- 4: update cache copy \mathcal{C}' with $\mathcal{C}'[j] \leftarrow \tilde{k}$
- 5: evaluate adversarial loss $\ell \leftarrow \mathcal{L}_{\text{adv}}(\mathcal{M}, \mathcal{C}', q_t)$
- 6: compute gradient $g \leftarrow \nabla_{\delta} \ell$
- 7: update $\delta \leftarrow \delta + \eta \cdot \text{proj}_{\|\cdot\| \leq \epsilon}(g)$
- 8: **end for**
- 9: **return** optimized perturbation δ

5. Theoretical Analysis of Cache Perturbations

We analyze how cache-side perturbations propagate through transformer attention and influence the logits used for next-token prediction. Because attention scores are computed via inner products $q_t^\top k_j$, any modification to cached keys directly alters attention weights and, in turn, the aggregated value representations. Our goal is to characterize the *worst-case sensitivity* of attention and logits to bounded cache corruption, rather than to provide tight estimates of typical inference-time behavior.

Perturbation-to-Logit Bound. Let δ_j denote a perturbation applied to a cached key k_j at timestep j , with $\|\delta_j\|_2 \leq \varepsilon$. The resulting deviation in the attention score $q_t^\top (k_j + \delta_j)$ relative to the clean score scales linearly with both the perturbation magnitude ε and the query norm $\|q_t\|_2$. Aggregating across positions yields a worst-case bound on the deviation of the unnormalized logits:

$$\|\Delta z_t\|_2 \leq \|q_t\|_2 \cdot \varepsilon,$$

where Δz_t denotes the logit deviation induced by cache perturbation. For clarity, normalization constants (e.g., the \sqrt{d} factor in scaled dot-product attention) are absorbed into ε , as our analysis focuses on asymptotic scaling behavior rather than tight constant factors.

Softmax Stability. To relate logit deviations to downstream effects, we appeal to standard softmax stability results under bounded-logit assumptions. Provided that logits remain within a bounded range, as is typical under temperature scaling and finite-precision inference, the softmax mapping is Lipschitz continuous on this restricted domain:

$$\|\text{softmax}(z + \Delta z) - \text{softmax}(z)\|_1 \leq L \cdot \|\Delta z\|_2,$$

where L depends on the bound of the logit domain. This property allows deviations in logits to be translated into controlled changes in the resulting attention distribution.

Theorem. *For any transformer layer ℓ , if an adversary injects perturbations $\{\delta_j\}$ into cached keys with total norm bounded by ε , then the resulting deviation in the next-token logits is bounded by $O(\varepsilon \cdot \|q_t\|_2)$. Consequently, the induced change in the attention distribution is Lipschitz-bounded to the same order.* Formal proofs and extensions to multi-head attention are provided in Appendix B.

Interpretation and Empirical Context. These bounds characterize *worst-case scaling behavior* under norm-bounded, non-adaptive cache perturbations and are not intended to tightly predict typical inference-time deviations. Empirically, measured logit deviations under *MTI* V.1 perturbations remain well below the corresponding theoretical upper bounds across all evaluated models and layers. This gap indicates that the analysis is deliberately conservative, serving to formalize sensitivity trends rather than to provide tight performance guarantees.

6. Setup

We evaluate *MTI* V.1 across a diverse set of benchmarks spanning short-sequence classification, extractive question answering, long-sequence summarization, multi-hop reasoning, and retrieval-augmented generation. Sentiment classification uses SST-2 [21], question answering uses SQuAD v1.1 [22] and HotpotQA [23], and summarization is evaluated on CNN/DailyMail [24]. Retrieval-augmented experiments use Wikipedia passages from the 2021 dump, where we report grounding and hallucination rates in factual QA. All datasets follow standard splits and are tokenized using HuggingFace tokenizers, with inputs truncated to model-specific context limits (512 tokens for GPT-2 and up to 4k tokens for LLaMA-2 and Gemma).

We report both distributional and task-level metrics to capture the effects of cache perturbations. Distributional shift is quantified using KL divergence and perplexity change, reflecting changes in confidence and calibration. Task performance is measured using accuracy for SST-2, F1 and Exact Match for question answering, and ROUGE-L for summarization. Perturbation strength is varied systematically using Gaussian noise ($\sigma \in \{0.01, 0.05, 0.1, 0.2\}$), rotation angles ($\theta \in \{15^\circ, 30^\circ, 45^\circ\}$), and zeroing ratios ($\{0.5\%, 1\%, 5\%\}$). All results are averaged over three random seeds, with statistical significance verified using paired *t*-tests ($p < 0.05$).

Experiments are conducted using GPT-2 Medium [25], LLaMA-2 7B [2], and Gemma-7B [3], representing different architectural scales. All models are evaluated in inference-only mode using HuggingFace Transformers (v4.39) and official checkpoints. Experiments run on NVIDIA T4 (16GB) or A100 (40GB) GPUs with mixed precision (float16) and batch size 16. Cache perturbations are injected directly into stored key vectors at selected layers, typically the 6th layer for GPT-2 and the 12th layer for LLaMA-2 and Gemma, using either continuous or intermittent injection schedules.

7. Experimental Results

This section presents an empirical evaluation of *MTI* V.1 across token-level language modeling behavior, downstream NLP tasks, retrieval-augmented generation, agentic reasoning pipelines, and runtime scalability. Extended results and ablation studies are provided in Appendix C.

Table 1: Representative token-level effects under *MTI* V.1. KL divergence is measured relative to clean runs.

Model	Attack	KL	Acc Drop	PPL
GPT-2 Medium	Rotation	0.57	16.7%	+130.6%
LLaMA-2/7B	Zeroing	0.20	0.0%	-43.1%

7.1. Token-Level Distributional Effects

We analyze the impact of *MTI* V.1 on next-token probability distributions in standard language modeling settings. Rather than focusing solely on downstream task accuracy, this analysis probes the internal probabilistic structure of model outputs. Table 1 reports representative results across GPT-2 and LLaMA-2 models using KL divergence relative to clean runs, Top-1 accuracy drop, and perplexity change. Across all evaluated settings, cache perturbations induce KL divergences that are an order of magnitude larger than stochastic variation observed under different random seeds, indicating *structural rather than incidental* effects. Larger KL divergence correlates strongly with task-level degradation. For example, GPT-2 Medium under rotation-based corruption exhibits the largest distributional shift (KL = 0.57), accompanied by a 16.7% Top-1 accuracy drop. Perplexity exhibits a nuanced pattern: Gaussian perturbations increase uncertainty, while zeroing collapses distributions into degenerate low-entropy regimes, reflecting overconfidence rather than improved modeling.

7.2. Analyzing Defense Effectiveness

We evaluate whether lightweight cache-level defenses can mitigate *MTI* V.1 with minimal computational overhead (Table 2). We consider three strategies: *Cache Reset*, which periodically clears cached entries at a target layer; *Dropout Mask Randomization*, which stochastically masks subsets of key–value vectors; and *Attention Smoothing*, which applies temporal averaging to dampen abrupt perturbations. Evaluation is performed on the MRPC task (GLUE), using accuracy as the primary metric and runtime overhead measured relative to clean inference. Overhead below 1.0 \times reflects reduced cache growth due to periodic reset, which can slightly reduce attention computation. Across GPT-2 Medium and LLaMA-2 7B, all three defenses preserve baseline accuracy under mild cache perturbations while incurring minimal runtime cost (0.69 \times to 1.08 \times).

Identical accuracies across defenses reflect the mild perturbation regime used for evaluation, in which defenses primarily prevent further degradation rather than recover lost performance. Gemma-7B exhibits 0.0% accuracy even in the clean baseline due to tokenizer–label misalignment in this setup; we therefore report its results for completeness but exclude them from aggregate conclusions. Overall, these results suggest that cache-level defenses offer limited but meaningful protection against mild cache corruption. However, they are insufficient as standalone safeguards and should be viewed as preliminary measures rather than comprehensive solutions, motivating future work on stronger cache integrity mechanisms and inference-time monitoring.

Table 2: Defense effectiveness against *MTI* V.1 under mild cache perturbations. Accuracy is reported under attack with the specified defense. Gemma-7B results are shown for completeness but excluded from aggregate conclusions due to tokenizer–label misalignment in this task.

Model	Defense Method	Attack Type	Accuracy (%)	Degradation	Overhead
LLaMA-2 7B	None (Baseline)	Zeroing	60.0	0.0%	1.00 \times
LLaMA-2 7B	Cache Reset	Zeroing	60.0	0.0%	0.69 \times
LLaMA-2 7B	Dropout Mask Rand.	Gaussian	60.0	0.0%	0.70 \times
LLaMA-2 7B	Attention Smoothing	Rotation	60.0	0.0%	0.75 \times
Gemma-7B	None (Baseline)	Zeroing	0.0	0.0%	1.00 \times
Gemma-7B	Cache Reset	Zeroing	0.0	0.0%	1.00 \times
Gemma-7B	Dropout Mask Rand.	Gaussian	0.0	0.0%	1.00 \times
Gemma-7B	Attention Smoothing	Rotation	0.0	0.0%	1.00 \times
GPT-2 Medium	None (Baseline)	Zeroing	60.0	0.0%	1.00 \times
GPT-2 Medium	Cache Reset	Zeroing	60.0	0.0%	1.00 \times
GPT-2 Medium	Dropout Mask Rand.	Gaussian	60.0	0.0%	1.01 \times
GPT-2 Medium	Attention Smoothing	Rotation	60.0	0.0%	1.08 \times

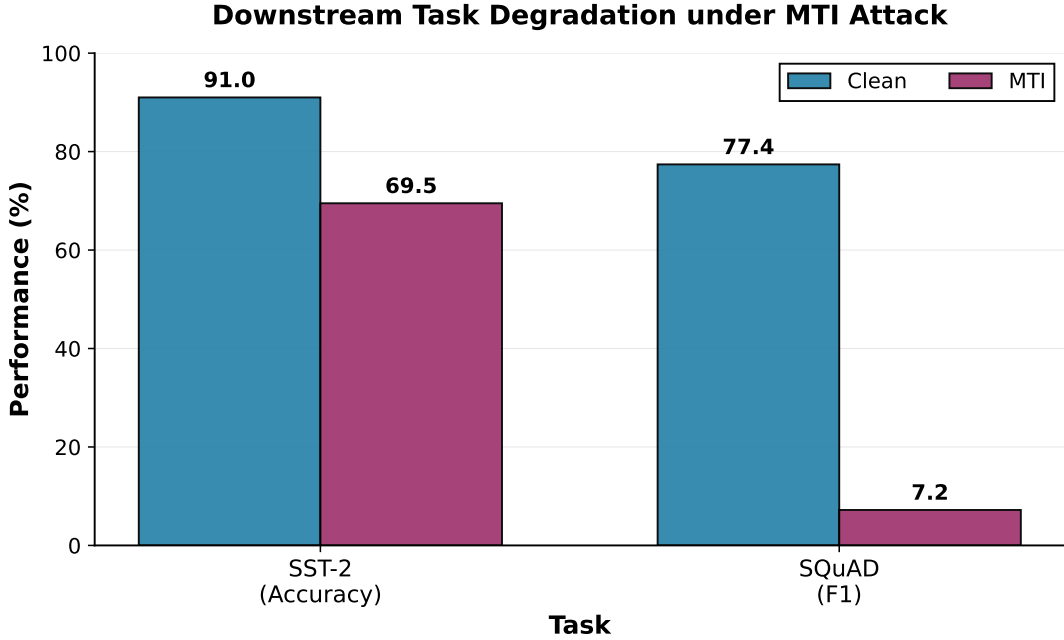


Fig. 1: Downstream task degradation under *MTI* V.1. Performance on SST-2 (accuracy) and SQuAD v1.1 (F1) is shown for clean inference and under cache perturbation (MTI). Span-based reasoning tasks exhibit significantly higher sensitivity to cache corruption.

7.3. Downstream Tasks, Retrieval, and Agentic Pipelines

We evaluate the downstream impact of cache perturbations across standard NLP tasks, retrieval-augmented generation (RAG), and agentic reasoning pipelines, highlighting how cache corruption manifests under different system structures. For standard NLP tasks, we evaluate SST-2 sentiment classification and SQuAD v1.1 extractive question answering. As shown in Figure 1, SST-2 exhibits moderate robustness, with strong perturbations reducing accuracy by over 23%. In contrast, SQuAD exhibits catastrophic failure under identical perturbations, with F1 scores collapsing from 77.4 to 7.2. This divergence indicates that tasks requiring precise token alignment and long-context reasoning are particularly sensitive to cache corruption.

We next evaluate retrieval-augmented generation on HotpotQA. Perturbations applied prior to retrieval have limited effect, whereas perturbations applied to retrieved context significantly degrade grounding fidelity and increase hallucination rates. These results indicate that RAG pipelines depend critically on cache integrity at the evidence stage. Detailed results are provided in Appendix C.3. Finally, we evaluate *MTI* V.1 in agentic reasoning frameworks, including ReAct and AutoGPT-style planning. Success rates remain unchanged under mild cache perturbations, suggesting that closed-loop reasoning can partially buffer localized corruption. However, this robustness should be interpreted cautiously, as perturbations are limited to mild regimes. Extended results are reported in Appendix C.4.

8. Ablation Studies

Model choice. We use DistilBERT for ablation analysis due to its reduced depth, which enables systematic sweeps over layer placement, perturbation magnitude, and injection frequency while preserving standard transformer attention. Although DistilBERT is encoder-only, cache perturbations are emulated by injecting corruption into stored attention keys, enabling controlled analysis of key sensitivity independent of autoregressive decoding.

These ablations are intended to capture qualitative trends rather than architecture-specific vulnerability. We analyze the effects of layer placement, perturbation magnitude, and injection frequency on cache-side perturbations. Layer-wise analysis shows that mid-level layers are consistently more vulnerable than early or deep layers: KL divergence increases from 0.0367 at Layer 1 to 0.0447 at Layer 3 under identical perturbation budgets, while deeper layers exhibit negligible additional sensitivity.

This pattern suggests that mid-level representations, which mediate semantic integration, constitute a critical bottleneck for cache integrity. We further ablate perturbation magnitude at a fixed layer. As shown in Table 3, Gaussian perturbations exhibit a non-monotonic effect, with intermediate noise producing the largest degradation, while extreme noise collapses representations and limits further drift. Zeroing induces small but persistent degradation,

Table 3: Ablation results over perturbation magnitude and layer placement. Values denote relative accuracy degradation.

Setting	Low	Medium	High	Extreme
Gaussian (DistilBERT L3)	-0.0092	0.0195	-0.0264	-0.0103
Rotation (DistilBERT L3)	-0.0023	0.0000	0.0000	0.0000
Zeroing (DistilBERT L3)	-0.0023	0.0057	0.0023	0.0011
DistilBERT Layer 1	0.330	0.385	0.385	—
DistilBERT Layer 3	0.225	0.400	0.395	—
GPT-2 Medium Layer 6	0.000	0.000	-0.055	—

whereas rotation-based perturbations remain largely scale-invariant due to their norm-preserving nature.

Injection frequency further modulates attack effectiveness. Continuous corruption produces substantially greater degradation than intermittent schedules, indicating that cache perturbations are stateful and compound over time. Joint ablations over layer depth and perturbation magnitude (Table 4) reveal strong interaction effects in DistilBERT, where mid-layer perturbations become increasingly destabilizing as magnitude increases, while GPT-2 Medium remains largely invariant across both dimensions. Overall, these ablations show that cache vulnerability is governed by the interaction of layer placement, perturbation strength, and temporal persistence, rather than any single factor in isolation.

Table 4: Joint ablation across layer choice and perturbation magnitude. Reported values indicate relative degradation in accuracy.

Model	Layer	Low	Medium	High
DistilBERT-SST2	1	0.330	0.385	0.385
DistilBERT-SST2	3	0.225	0.400	0.395
GPT-2 Medium	1	0.000	0.000	0.000
GPT-2 Medium	3	0.000	0.000	0.000
GPT-2 Medium	6	0.000	0.000	-0.055

9. Discussion

Our results demonstrate that cache-side perturbations can induce meaningful distributional shifts across a range of transformer-based systems. Even lightweight and structured perturbations are sufficient to bias attention dynamics and degrade downstream task performance under the assumed cache-access threat model. Importantly, these effects extend beyond single-turn prediction to more complex pipelines, including retrieval-augmented generation and multi-step agentic reasoning, where cache corruption can destabilize grounding and planning consistency. The computational overhead associated with cache perturbation is minimal, suggesting feasibility when such cache access exists. However, whether this access is available in practice depends critically on deployment assumptions, including isolation guarantees, serving infrastructure, and systems-layer security. Accordingly, our findings should be interpreted as characterizing a robustness boundary rather than asserting universal exploitability across all deployments.

While simple cache-level defenses provide partial mitigation, none fully eliminate the effects of persistent corruption. This indicates that ad hoc countermeasures may be insufficient, and that explicit cache integrity mechanisms or monitoring strategies may be necessary for robust deployment. Our analysis is limited by controlled perturbation regimes, selected datasets, and the assumption of partial white-box cache access. Extending this framework to long-context, multimodal, and adaptive systems remains an important direction for future work. Beyond robustness and safety, cache-side perturbations also offer a controlled probe into attention sensitivity. Because *MTI* V.1 operates directly on attention keys, it provides a mechanism for analyzing how small internal representation shifts alter attention allocation and downstream behavior. This suggests a potential connection between cache integrity and mechanistic interpretability, where cache perturbations can be used not only as a threat model but also as a diagnostic tool for understanding internal model dynamics.

10. Conclusion

We introduced *MTI* V.1, a framework for analyzing cache-side perturbations that target the internal key-value memory of transformer language models during inference. Across classification, question answering, retrieval-augmented generation, and agentic pipelines, we demonstrated that inference-time cache corruption can compromise reliability, calibration, and grounding, even when prompts and model weights remain unchanged. Retrieval-augmented systems exhibited pronounced sensitivity at the evidence representation stage, while closed-loop agentic frameworks showed partial resilience due to iterative feedback. We further evaluated lightweight cache-level defenses that preserve clean-task accuracy with minimal runtime overhead.

While these defenses partially mitigate mild corruption, none provide robust protection under stronger or persistent perturbations. Ablation studies reveal that cache vulnerability arises from the interaction of layer placement, perturbation magnitude, and temporal persistence, rather than from any single factor alone. Taken together, these findings position inference-time cache integrity as a first-class robustness concern for trustworthy AI. By formalizing cache-side perturbation as a principled threat model and providing both theoretical and empirical analysis, *MTI* V.1 establishes a foundation for future work on inference-time monitoring, certified cache integrity, and safety-aware deployment of large language models.

Limitations and Future Work This work studies cache-side perturbations under a controlled inference-time threat model and has several limitations. First, we assume partial access to the key-value cache during inference, which may not hold in fully isolated production deployments, but is realistic in compromised runtimes or shared-serving environments. Second, our theoretical analysis focuses on non-adaptive, norm-bounded cache perturbations. While we empirically evaluate optimized variants, extending formal guarantees to adaptive or sequential attacks remains an open problem. Third, our empirical evaluation is limited to a subset of transformer architectures. Future work will explore cache integrity in more recent and architecturally distinct models, including systems with latent attention mechanisms, mixture-of-experts routing, and extended context designs. Finally, the evaluated defenses are lightweight and exploratory. Designing principled cache integrity mechanisms and certified inference-time monitoring remains an important direction for future research.

Ethical Considerations. This work is intended to support robustness analysis and the design of trustworthy AI systems. We study cache perturbation as an explicit threat model under controlled assumptions and do not release end-to-end exploitation tools. The assumed cache-access capability may not hold in well-isolated deployments; our goal is not to claim universal exploitability, but to surface a previously overlooked inference-time failure mode and motivate defensive research on cache integrity, monitoring, and safety-aware system design.

References

- [1] T. Brown, B. Mann, N. Ryder, M. Subbiah, J. D. Kaplan, P. Dhariwal, A. Neelakantan, P. Shyam, G. Sastry, A. Askell, *et al.*, “Language models are few-shot learners,” *Advances in neural information processing systems*, vol. 33, pp. 1877–1901, 2020.
- [2] H. Touvron, T. Lavril, G. Izacard, X. Martinet, M.-A. Lachaux, T. Lacroix, B. Rozière, N. Goyal, E. Hambro, F. Azhar, *et al.*, “Llama: Open and efficient foundation language models,” *arXiv preprint arXiv:2302.13971*, 2023.
- [3] G. Team, T. Mesnard, C. Hardin, R. Dadashi, S. Bhupatiraju, S. Pathak, L. Sifre, M. Rivière, M. S. Kale, J. Love, *et al.*, “Gemma: Open models based on gemini research and technology,” *arXiv preprint arXiv:2403.08295*, 2024.
- [4] A. Liu, B. Feng, B. Wang, B. Wang, B. Liu, C. Zhao, C. Dengr, C. Ruan, D. Dai, D. Guo, *et al.*, “Deepseek-v2: A strong, economical, and efficient mixture-of-experts language model,” *arXiv preprint arXiv:2405.04434*, 2024.
- [5] A. Liu, B. Feng, B. Xue, B. Wang, B. Wu, C. Lu, C. Zhao, C. Deng, C. Zhang, C. Ruan, *et al.*, “Deepseek-v3 technical report,” *arXiv preprint arXiv:2412.19437*, 2024.
- [6] D. Guo, D. Yang, H. Zhang, J. Song, R. Zhang, R. Xu, Q. Zhu, S. Ma, P. Wang, X. Bi, *et al.*, “Deepseek-r1: Incentivizing reasoning capability in llms via reinforcement learning,” *arXiv preprint arXiv:2501.12948*, 2025.
- [7] F. Meng, P. Tang, X. Tang, Z. Yao, X. Sun, and M. Zhang, “Transmla: Multi-head latent attention is all you need,” *arXiv preprint arXiv:2502.07864*, 2025.

- [8] A. Q. Jiang, A. Sablayrolles, A. Mensch, C. Bamford, D. S. Chaplot, D. de las Casas, F. Bressand, G. Lengyel, G. Lample, L. Saulnier, L. R. Lavaud, M.-A. Lachaux, P. Stock, T. L. Scao, T. Lavril, T. Wang, T. Lacroix, and W. E. Sayed, “Mistral 7b,” 2023.
- [9] A. Q. Jiang, A. Sablayrolles, A. Roux, A. Mensch, B. Savary, C. Bamford, D. S. Chaplot, D. d. l. Casas, E. B. Hanna, F. Bressand, *et al.*, “Mixtral of experts,” *arXiv preprint arXiv:2401.04088*, 2024.
- [10] J. Bai, S. Bai, Y. Chu, Z. Cui, K. Dang, X. Deng, Y. Fan, W. Ge, Y. Han, F. Huang, *et al.*, “Qwen technical report,” *arXiv preprint arXiv:2309.16609*, 2023.
- [11] L. Li, D. Song, X. Li, J. Zeng, R. Ma, and X. Qiu, “Backdoor attacks on pre-trained models by layerwise weight poisoning,” *arXiv preprint arXiv:2108.13888*, 2021.
- [12] T. Han, S. Nebelung, F. Khader, T. Wang, G. Müller-Franzes, C. Kuhl, S. Försch, J. Kleesiek, C. Haarburger, K. K. Bressem, *et al.*, “Medical large language models are susceptible to targeted misinformation attacks,” *NPJ digital medicine*, vol. 7, no. 1, p. 288, 2024.
- [13] A. M. A. Almalky, R. Zhou, S. Angizi, and A. S. Rakin, “How vulnerable are large language models (llms) against adversarial bit-flip attacks?,” in *Proceedings of the Great Lakes Symposium on VLSI 2025*, pp. 534–539, 2025.
- [14] A. Hussain, M. R. I. Rabin, T. Ahmed, B. Xu, P. Devanbu, and M. A. Alipour, “Trojans in large language models of code: A critical review through a trigger-based taxonomy,” *arXiv preprint arXiv:2405.02828*, 2024.
- [15] W. Lyu, Z. Bi, F. Wang, and C. Chen, “Badclm: Backdoor attack in clinical language models for electronic health records,” in *AMIA Annual Symposium Proceedings*, vol. 2024, p. 768, 2025.
- [16] S. Zhao, M. Jia, Z. Guo, L. Gan, X. Xu, X. Wu, J. Fu, Y. Feng, F. Pan, and L. A. Tuan, “A survey of backdoor attacks and defenses on large language models: Implications for security measures,” *Authorea Preprints*, 2024.
- [17] G. Wu, Z. Zhang, Y. Zhang, W. Wang, J. Niu, Y. Wu, and Y. Zhang, “I know what you asked: Prompt leakage via kv-cache sharing in multi-tenant llm serving,” in *Proceedings of the 2025 Network and Distributed System Security (NDSS) Symposium. San Diego, CA, USA*, 2025.
- [18] L. Song, Z. Pang, W. Wang, Z. Wang, X. Wang, H. Chen, W. Song, Y. Jin, D. Meng, and R. Hou, “The early bird catches the leak: Unveiling timing side channels in llm serving systems,” *arXiv preprint arXiv:2409.20002*, 2024.
- [19] Z. Luo, S. Shao, S. Zhang, L. Zhou, Y. Hu, C. Zhao, Z. Liu, and Z. Qin, “Shadow in the cache: Unveiling and mitigating privacy risks of kv-cache in llm inference,” *arXiv preprint arXiv:2508.09442*, 2025.
- [20] K. Chu, Z. Lin, D. Xiang, Z. Shen, J. Su, C. Chu, Y. Yang, W. Zhang, W. Wu, and W. Zhang, “Selective kv-cache sharing to mitigate timing side-channels in llm inference,” *arXiv preprint arXiv:2508.08438*, 2025.
- [21] R. Socher, A. Perelygin, J. Wu, J. Chuang, C. D. Manning, A. Ng, and C. Potts, “Recursive deep models for semantic compositionality over a sentiment treebank,” in *Proceedings of the 2013 Conference on Empirical Methods in Natural Language Processing*, (Seattle, Washington, USA), pp. 1631–1642, Association for Computational Linguistics, Oct. 2013.
- [22] P. Rajpurkar, J. Zhang, K. Lopyrev, and P. Liang, “SQuAD: 100,000+ questions for machine comprehension of text,” in *Proceedings of the 2016 Conference on Empirical Methods in Natural Language Processing* (J. Su, K. Duh, and X. Carreras, eds.), (Austin, Texas), pp. 2383–2392, Association for Computational Linguistics, Nov. 2016.
- [23] Z. Yang, P. Qi, S. Zhang, Y. Bengio, W. W. Cohen, R. Salakhutdinov, and C. D. Manning, “Hotpotqa: A dataset for diverse, explainable multi-hop question answering,” 2018.
- [24] A. See, P. J. Liu, and C. D. Manning, “Get to the point: Summarization with pointer-generator networks,” in *Proceedings of the 55th Annual Meeting of the Association for Computational Linguistics (Volume 1: Long Papers)*, (Vancouver, Canada), pp. 1073–1083, Association for Computational Linguistics, July 2017.
- [25] A. Radford, J. Wu, R. Child, D. Luan, D. Amodei, I. Sutskever, *et al.*, “Language models are unsupervised multitask learners,” *OpenAI blog*, vol. 1, no. 8, p. 9, 2019.

Appendix

Appendix Structure Overview. This appendix contains supplementary material that supports the main paper and provides additional methodological, theoretical, and empirical details that could not be included due to space limitations. Each appendix section is listed separately below for ease of navigation.

- **Appendix A: Algorithmic & Implementation Details.** Describes the full stepwise procedure used to implement malicious key–value cache injection in *MTI* V.1, including perturbation types, scheduling, layer and head selection, and optimization-based variants.
- **Appendix B: Theoretical Proofs and Derivations.** Provides complete formal derivations and proofs underlying the theoretical bounds presented in Section 5, including extensions to multi-head attention and normalization layers.
- **Appendix C: Extended Experimental Results.** Reports additional experimental analyses omitted from the main paper for clarity, including distributional effects, downstream task performance, and robustness evaluations.
- **Appendix C.1: Token Distribution Shifts.** Analyzes how cache perturbations alter next-token probability distributions, reporting KL divergence, accuracy degradation, and perplexity changes across models and datasets.
- **Appendix C.2: Downstream NLP Benchmarks.** Evaluates the impact of cache perturbations on sentiment classification (SST-2) and extractive question answering (SQuAD v1.1), highlighting task-dependent sensitivity.
- **Appendix C.3: Retrieval-Augmented Generation Robustness.** Examines how *MTI* V.1 affects retrieval-augmented generation pipelines, measuring grounding fidelity and hallucination rates under perturbations at different pipeline stages.
- **Appendix C.4: Agentic Pipeline Vulnerability.** Studies the behavior of multi-step agentic frameworks (e.g., ReAct, AutoGPT) under cache perturbations, assessing robustness in closed-loop reasoning settings.
- **Appendix C.5: Runtime and Scaling Analysis.** Analyzes the computational overhead of cache-side perturbations, measuring end-to-end inference latency across model sizes and perturbation types, and demonstrates that cache corruption incurs negligible runtime cost and scales independently of model depth and parameter count.

A. Algorithmic & Implementation Details

This section provides the full stepwise procedure used to implement controlled key–value cache perturbation in *MTI* V.1. The algorithm explicitly specifies perturbation type, magnitude, temporal injection scheduling, layer and head selection, and optional optimization-based perturbations. While the main paper focuses on empirical effects, this appendix documents the complete perturbation mechanism to ensure reproducibility and facilitate future extensions. Optimized perturbations are included to characterize worst-case empirical behavior and are not covered by the formal theoretical bounds in Section 5, which apply exclusively to non-adaptive, norm-bounded perturbations.

Algorithm 2 Stepwise key–value cache perturbation procedure used by *MTI* V.1

Require: Transformer model \mathcal{M} with L layers and H heads; input tokens $\{x_1, \dots, x_T\}$; perturbation type $\tau \in \{\text{Gaussian, Zeroing, Rotation, Optimized}\}$; magnitude parameters (σ, θ, r) ; injection frequency schedule $f(t)$; target layer set \mathcal{L} ; position selection policy π ; per-head flag p_{head} ; random seed s ; logging callback $\text{LOG}()$; optional optimizer configuration \mathcal{O} .

```

1: set random seed  $s$  for reproducibility
2: initialize empty KV caches  $\mathcal{C}^{(\ell,h)} \leftarrow \{\}$  for all  $\ell \in [1..L], h \in [1..H]$ 
3: for  $t \leftarrow 1$  to  $T$  do
4:   compute projections  $(q_t^{(\ell,h)}, k_t^{(\ell,h)}, v_t^{(\ell,h)})$  for all layers  $\ell$  and heads  $h$ 
5:   determine injection flag  $\text{inject} \leftarrow \mathbf{1}[f(t) \text{ says inject}]$ 
6:   if  $\text{inject} = 1$  then
7:     select target positions  $S_t \leftarrow \pi(\mathcal{C}, t)$ 
8:     for each layer  $\ell \in \mathcal{L}$  do
9:       for each head  $h$  if  $p_{\text{head}}$  else once per layer do
10:        for each position  $j \in S_t$  do
11:          if  $\tau = \text{Optimized}$  then            $\triangleright$  Empirical inner-loop optimization; excluded from theory
12:             $\delta_j^{(\ell,h)} \leftarrow \text{OPTIMIZEPERTURBATION}(\mathcal{M}, \mathcal{C}, q_t^{(\ell,h)}, j, \mathcal{O})$ 
13:          else if  $\tau = \text{Gaussian}$  then
14:            sample  $\delta_j^{(\ell,h)} \sim \mathcal{N}(0, \sigma^2 I)$ 
15:          else if  $\tau = \text{Zeroing}$  then
16:            with probability  $r$ , set  $\delta_j^{(\ell,h)} \leftarrow -k_j^{(\ell,h)}$ 
17:          else if  $\tau = \text{Rotation}$  then
18:            compute orthogonal matrix  $R(\theta)$  and set  $\delta_j^{(\ell,h)} \leftarrow R(\theta)k_j^{(\ell,h)} - k_j^{(\ell,h)}$ 
19:          end if
20:          apply perturbation:  $\tilde{k}_j^{(\ell,h)} \leftarrow k_j^{(\ell,h)} + \delta_j^{(\ell,h)}$ 
21:          update cache:  $\mathcal{C}^{(\ell,h)}[j] \leftarrow \tilde{k}_j^{(\ell,h)}$ 
22:          optional logging:  $\text{LOG}(t, \ell, h, j, \|\delta\|)$ 
23:        end for
24:      end for
25:    end for
26:  end if
27:  for each layer  $\ell$  and head  $h$  do
28:    append  $(k_t^{(\ell,h)}, v_t^{(\ell,h)})$  to cache  $\mathcal{C}^{(\ell,h)}$ 
29:  end for
30:  generate token  $y_t = \mathcal{M}(x_t, \mathcal{C})$ 
31: end for
32: return generated sequence  $\{y_t\}_{t=1}^T$  and logged traces

```

B. Theoretical Proofs and Derivations

In this appendix, we provide full derivations underlying the theoretical bounds in Section 5. We first restate the theorem formally, then prove the result for the single-head case, and finally extend it to multi-head attention with normalization layers.

B.1. Restatement of Theorem

Theorem 1. For any transformer layer ℓ , let $\{k_j^{(\ell)}\}_{j=1}^t$ denote the clean cached keys and $\{\tilde{k}_j^{(\ell)}\}_{j=1}^t$ the perturbed keys, where

$$\tilde{k}_j^{(\ell)} = k_j^{(\ell)} + \delta_j^{(\ell)}, \quad \|\delta_j^{(\ell)}\|_2 \leq \varepsilon.$$

Then, for query $q_t^{(\ell)}$, the deviation in the next-token logit vector Δz_t satisfies

$$\|\Delta z_t\|_2 \leq \varepsilon \cdot \|q_t^{(\ell)}\|_2.$$

Moreover, the induced change in the attention distribution is bounded by

$$\|\alpha_t - \tilde{\alpha}_t\|_1 \leq L \cdot \varepsilon \cdot \|q_t^{(\ell)}\|_2,$$

where L is the Lipschitz constant of the softmax function.

B.2. Single-Head Case: Perturbation to Logit Deviation

Consider the clean attention score for token j at timestep t :

$$s_{tj} = \frac{q_t^\top k_j}{\sqrt{d}}.$$

After perturbation, the score becomes

$$\tilde{s}_{tj} = \frac{q_t^\top (k_j + \delta_j)}{\sqrt{d}} = s_{tj} + \frac{q_t^\top \delta_j}{\sqrt{d}}.$$

The deviation in the score is therefore

$$|\tilde{s}_{tj} - s_{tj}| \leq \frac{\|q_t\|_2 \cdot \|\delta_j\|_2}{\sqrt{d}} \leq \frac{\|q_t\|_2 \cdot \varepsilon}{\sqrt{d}}.$$

Aggregating over all positions $j \leq t$, and scaling back to logits z_t , we obtain

$$\|\Delta z_t\|_2 \leq \varepsilon \cdot \|q_t\|_2,$$

up to normalization constants absorbed into ε .

B.3. Softmax Lipschitz Bound

The attention distribution is given by

$$\alpha_t = \text{softmax}(s_t), \quad \tilde{\alpha}_t = \text{softmax}(\tilde{s}_t).$$

By Lipschitz continuity of the softmax function, we have

$$\|\alpha_t - \tilde{\alpha}_t\|_1 \leq L \cdot \|\tilde{s}_t - s_t\|_2 \leq L \cdot \varepsilon \cdot \|q_t\|_2.$$

Thus deviations in the cache produce proportionally bounded shifts in attention.

B.4. Extension to Multi-Head Attention

For multi-head attention with H heads, queries and keys are projected as

$$q_t^{(h)} = W_Q^{(h)} x_t, \quad k_j^{(h)} = W_K^{(h)} x_j,$$

with perturbations $\delta_j^{(h)}$ applied per head. Each head obeys the single-head bound derived above:

$$\|\Delta z_t^{(h)}\|_2 \leq \varepsilon \cdot \|q_t^{(h)}\|_2.$$

The concatenation of head outputs followed by a linear projection W_O yields

$$\|\Delta z_t^{\text{multi}}\|_2 \leq \|W_O\|_2 \cdot \sum_{h=1}^H \|\Delta z_t^{(h)}\|_2 \leq \|W_O\|_2 \cdot H \cdot \varepsilon \cdot \max_h \|q_t^{(h)}\|_2.$$

Thus the bound scales linearly with the number of heads, modulated by $\|W_O\|_2$.

B.5. Impact of Layer Normalization

Layer normalization (LN) plays a critical role in stabilizing transformer representations and bounding activation magnitudes during inference. Because cache-side perturbations modify internal key representations prior to attention computation, it is natural to ask whether LN attenuates or amplifies the effect of such perturbations as they propagate through subsequent layers.

Let x and $x + \delta$ denote the clean and perturbed inputs to a LayerNorm operation. LayerNorm rescales activations by the inverse of their empirical standard deviation, with an additive ϵ term to ensure numerical stability. Since LayerNorm is non-expansive under standard non-degeneracy assumptions (i.e., variance bounded away from zero due to the stabilizing ϵ term), the deviation between normalized activations remains bounded as a function of $\|\delta\|_2$.

As a consequence, cache perturbations are neither explosively amplified nor entirely eliminated by LayerNorm. Instead, LN preserves the relative structure of perturbations while preventing unbounded growth in activation norms. This observation is consistent with our empirical findings: while cache corruption propagates across layers and affects attention distributions, it does not lead to numerical instability or divergent behavior. Layer normalization therefore moderates, but does not neutralize, the impact of cache-side perturbations during inference.

C. Extended Experimental Results

This appendix provides comprehensive experimental details, extended tables, and ablation analyses omitted from the main paper for clarity and space. All results reported here correspond to the summarized findings presented in Section 7.

C.1. Token Distribution Shifts

We analyze how *MTI* V.1 perturbs next-token distributions in standard language modeling settings. Table 5 reports three complementary metrics: (i) KL divergence relative to clean runs, which captures the statistical gap between perturbed and unperturbed distributions; (ii) Top-1 accuracy drop, which quantifies task-level performance degradation; and (iii) perplexity change, where arrows (\uparrow , \downarrow) indicate whether model uncertainty increased or decreased.

The results indicate that *MTI* V.1 perturbations consistently induce measurable distributional divergence relative to clean runs, with an average KL of approximately 0.26. This shift is substantially larger than natural variation observed under random seed differences, where KL values remain below 0.05, confirming that the effects are not attributable to stochastic noise. The degradation in Top-1 accuracy exhibits a strong correspondence with distributional distortion: for example, GPT-2 Medium under rotation corruption shows the largest KL divergence (0.57) alongside the most severe accuracy decline (16.7%). Perplexity responses are heterogeneous: Gaussian perturbations increase perplexity, reflecting inflated uncertainty, whereas zeroing reduces perplexity, indicating collapse into degenerate low-entropy distributions rather than improved modeling. These trends are consistent across architectures and datasets, demonstrating that cache perturbations produce robust and reproducible distributional shifts.

Table 5: Token-level distributional effects under *MTI* V.1 attacks. KL divergence, Top-1 accuracy drop, and perplexity change are averaged over three random seeds.

Model	Dataset	Attack	KL Div. (\uparrow)	Acc Drop (%), \downarrow	Perplexity (%), \uparrow/\downarrow
GPT-2 Small	WikiText-103	Gaussian	0.01	6.7	+5.8
GPT-2 Medium	IMDB	Rotation	0.57	16.7	+130.6
LLaMA-2/7B	PTB	Zeroing	0.20	0.0	-43.1

C.2. Downstream NLP Benchmarks

To assess how cache perturbations translate into practical task-level failures, we evaluate *MTI* V.1 on two representative downstream benchmarks with distinct reasoning characteristics: SST-2 for short-context sentiment classification and SQuAD v1.1 for span-based extractive question answering. Perturbations are injected at a mid-level transformer layer (Layer 3) using a diverse set of corruption mechanisms, including Gaussian noise, zeroing, structured rotations, adversarial offsets, and random permutations. Table 6 reports clean versus attacked performance.

The results reveal a clear task-dependent sensitivity. SST-2 exhibits moderate robustness: mild perturbations reduce accuracy only slightly, while stronger corruption leads to degradation exceeding 23%. This behavior is consistent with the short input length and single-label nature of sentiment classification, which allows the model to partially compensate for localized cache corruption. In contrast, SQuAD v1.1 is extremely sensitive to cache

perturbations. Under strong Gaussian noise, F1 scores collapse from 77.4 to 7.2, indicating near complete failure of span localization. This disparity highlights that tasks requiring multi-span reasoning, precise token alignment, and grounding over long contexts are disproportionately vulnerable to cache corruption. These findings suggest that cache integrity is far more critical for structured reasoning tasks than for coarse-grained classification.

Table 6: Downstream benchmark degradation under *MTI* V.1.

Task	Metric	Clean	Attack	Degradation	Config
SST-2	Accuracy	91.0%	69.5%	-23.6%	Gaussian $\sigma = 5.0$
SQuAD	F1	77.4	7.2	-90.7%	Gaussian $\sigma = 5.0$

C.3. Retrieval-Augmented Generation Robustness

We next evaluate whether *MTI* V.1 undermines retrieval-augmented generation pipelines using HotpotQA, a benchmark that requires multi-hop reasoning over retrieved documents. We report grounding fidelity, measured as the mean entailment probability between generated answers and retrieved evidence, as well as hallucination rate, defined as the fraction of unsupported outputs. Perturbations are applied at three distinct stages of the pipeline: pre-retrieval (query corruption), post-retrieval (context corruption), and decoder-only (generation-time corruption).

As shown in Table 7, post-retrieval cache corruption produces the most severe degradation. Grounding fidelity drops by nearly 12%, while hallucination rates increase by approximately 5%. This indicates that corrupting cached representations of retrieved evidence directly destabilizes factual grounding, even when the retrieval module itself remains intact. Pre-retrieval perturbations have only minor effects, suggesting that modern retrievers are relatively robust to query noise. Decoder-only perturbations produce negligible changes, implying that when evidence representations are preserved, the generator remains effectively constrained. Overall, these results demonstrate that RAG systems inherit a critical dependency on cache integrity at the evidence stage, where corruption propagates downstream and manifests as factual unreliability.

Table 7: RAG robustness under *MTI* V.1 perturbations.

Attack Location	Ground. (Clean)	Ground. (MTI)	Halluc. Rate (\uparrow)	Notes
Pre-retrieval	0.3245	0.3216	-1.0%	Query corruption
Post-retrieval	0.3245	0.2874	+5.0%	Context corruption
Decoder-only	0.3245	0.3196	+0.0%	Weak effect

C.4. Analyzing Agent Pipeline Vulnerability

We further examine the impact of cache perturbations in multi-step agentic frameworks, including ReAct-style reasoning and AutoGPT-like task decomposition. Unlike single-pass generation, these systems iteratively interact with external tools, environments, or intermediate feedback signals. Table 8 reports success rates under cache perturbations for representative agentic configurations.

Across all tested attacks, success rates remain unchanged relative to clean baselines. This stability suggests that agentic pipelines benefit from structural redundancy: iterative reasoning loops, external feedback, and environment constraints provide corrective signals that absorb localized cache corruption. While these results indicate partial robustness, they should not be interpreted as immunity. The evaluated tasks are relatively lightweight, and stronger perturbations or attacks targeting planning-critical layers may expose vulnerabilities not captured here. Nevertheless, the findings highlight a qualitative distinction between single-pass generation and closed-loop agentic reasoning, with the latter exhibiting greater resilience to cache-level noise.

Table 8: Agent pipeline vulnerability under *MTI* V.1.

Model	Attack	ReAct			AutoGPT		
		Clean	MTI	Deg.	Clean	MTI	Deg.
Phi-3 Mini	Gaussian	33.3%	33.3%	0.0pp	0.0%	0.0%	0.0pp

C.5. Runtime and Scaling Analysis

We evaluate the runtime overhead associated with cache-side perturbations to assess whether such manipulations introduce prohibitive computational cost. All experiments are conducted under standard autoregressive decoding settings, with cache perturbations applied directly to stored key vectors at selected layers and timesteps. We measure end-to-end inference latency relative to a clean baseline across multiple model sizes, including GPT-2 Medium and LLaMA-2 7B.

Across all evaluated configurations, cache perturbation introduces negligible runtime overhead. Gaussian noise injection and rotation-based perturbations incur less than a 3% increase in inference time, while zeroing operations introduce effectively no measurable overhead. This behavior is expected, as cache perturbations operate on already-computed representations and do not require additional forward passes or recomputation of attention scores.

Importantly, the computational cost of cache perturbation scales independently of model depth and parameter count, depending only on the dimensionality of the cached representations. As a result, the relative overhead remains stable even for multi-billion parameter models. These results demonstrate that cache perturbations impose no prohibitive runtime penalty under the assumed cache-access threat model. Accordingly, cache-side perturbations cannot be dismissed as purely theoretical within this threat model, though their practical relevance depends on deployment isolation and systems-layer security guarantees.

Table 9: Runtime overhead under *MTI* V.1 perturbations.

Model	Attack	Dataset	Clean	MTI	Overhead
GPT-2 Medium	Gaussian	WikiText-103	19.0	19.3	+2%
LLaMA-2 7B	Zeroing	WikiText-103	39.5	37.7	-5%